Analysis of Creep Behavior of a High Rockfill Dam

Y. Delavar Rafie[a], A. Maddah[a*], A. Soroush[a]

[a] Department of Civil and Environmental Engineering, Amirkabir University of Technology (Tehran Polytechnic), Tehran, Iran, 159163-4311.

* *Corresponding author:*
arman_maddah@aut.ac.ir
+982164543001

Abstract

Rockfill materials experience gradual deformation over time, which can cause serious problems in rockfill structures, especially in dams. This deformation may lead to reduced confinement of the dam core by the shells, resulting in large deformations within the dam body, as well as cracking in filters and core, a loss of freeboard, and damage to associated facilities. The creep behavior of rockfill materials is influenced by various factors, such as stress level, material composition, aggregate shape, particle size, and moisture content. This study presents the application of the Soft Soil Creep model to simulate both volumetric and shear creep in rockfill materials. The model parameters were determined from large-scale oedometer tests using an integrated procedure that combines experimental data with numerical back-analysis, ensuring a physically consistent parameter set. Furthermore, the study analyzes the influence of these parameters on rockfill

behavior, highlighting their role in controlling the creep deformations. As a case study, the creep behavior of the rockfill shells in the 177-m-high Masjed Soleyman Dam is investigated. The study confirms the model reliability in predicting dam settlement patterns through comparison with measured data and observations. Localized computed shear strain in upper level of the dam exceeded 50 % aligning with what accrued in the prototype.

Keywords: Creep, Rockfill, Masjed Soleyman Dam, Soft Soil Creep Model, Numerical Analysis

1. Introduction

Rockfills are coarse-grained materials, with high shear strength and significant permeability. Due to the availability of rockfill materials in nature, their ability to absorb seismic loads and their adaptability to various resistance and deformability conditions, they are utilized in earth-rockfill dams and rockfill concrete dams (RCD), airport subgrades, foundations of large industrial structures, and ground improvement projects. Moreover, the accessibility to heavy machinery along with economic feasibility have led to increased use of rockfill materials.

One of the significant characteristics of rockfill materials is their time-dependent creep displacement, which is influenced by several factors such as stress level and directions, material composition, aggregate shape, particle size, and moisture

content [1-11]. Creep deformations in rockfill structures in case of exceeding allowable limits, can disrupt the performance of the structure. For instance, the Atatürk Dam in Turkey, the Cechena Dam in Australia, and the TSQ-1 Dam in China have shown significant long-term settlements [12-15].

While the long-term dam deformations are affected by factors beyond creep, such as rockfill softening due to water infiltration, weathering caused by wet-dry cycles, and reservoir water level fluctuations, a substantial share of these deformations is linked to creep and its influencing factors. Therefore, given the importance of dams and their performance, it is essential to properly assess and consider the creep phenomenon in rockfill dams, predict deformations and ensure their safety to prevent excessive deformations.

Creep is the deformation of materials under constant stress over time, which consists of three phases (

Figure **Captions**

Figure *1*). Depending on the applied volumetric or shear stress, it can be classified into two types: volumetric creep and shear creep. Generally, volumetric creep occurs in the first phase, while shear creep, depending on the magnitude of the shear stress, can occur in any of the three creep phases [16].

Several constitutive models have been developed for modeling the creep of rockfill materials. These models can generally be divided into two categories: rheological models and empirical models [17]. Rheological models are derived from the combination of simple mechanical models such as elastic springs, plastic elements, and Newtonian ideal viscous fluid elements. Several rheological models are developed to model creep behavior in rockfills [18,19]. The Burger model is one of the common rheological models used in rockfill creep modeling. The Burger model is created by combining the Kelvin and Maxwell models in series. The Kelvin model, consisting of a spring and a dashpot arranged in parallel, represents elastic deformation with a time delay, effectively simulating the initial phase of creep. The Maxwell model, on the other hand, is the result of combining a spring and a dashpot in series and models the initial elastic deformation and the steady-state viscous flow. The Burger model does not simulate the third phase of creep (

Figure **Captions**

Figure *1*) and volumetric creep [20].

Empirical models are derived from laboratory data analysis, defining a functional relationship to represent creep. One such example is an elastoplastic creep model based on a power function, which was developed to assess the creep behavior of the

Shibuya Dam during both its construction and operational periods [21]. In recent decades, several other models have also been proposed to estimate the stress-strain behavior of rockfill materials using numerical simulation [22-30]. The Hardening Soil (HS) model is one of the widely used models for simulating the characteristics of rockfill materials. It is generated based on elastoplasticity theory with double yield surfaces. Originally designed for soil behavior, this model lacked the capability to simulate creep in rockfill materials, prompting several modifications to make it suitable for such applications. The modifications involve modeling substantial volumetric changes under high stress conditions and integrating the influence of particle breakage [31, 32]. Additionally, some of the proposed models for creep modeling are based on the Discrete Element Method (DEM), which allows for more detailed simulations but include high computational costs, especially for large structures such as dams [1, 33- 34].

Most current models for calculating creep in rockfill materials often rely on complex equations that are not available as built-in features in engineering software. Furthermore, a significant limitation of these models is their inability to concurrently simulate both volumetric and shear creeps, resulting in reduced accuracy and an incomplete representation of the true mechanical response of rockfill materials. Thus, there is a clear need for a model that overcomes these limitations and enables a more comprehensive analysis of rockfill material behavior. This study investigates

the capability of Soft Soil Creep (SSC) model, which features fewer parameters, is built into software, and considers both shear and volumetric creep, for simulating the rockfill material creep behavior.

2. Soft Soil Creep Model

The Soft Soil Creep (SSC) model is a constitutive model specifically developed to capture the time-dependent behavior of soft soils under long-term loading conditions. This model is an extension of the Soft Soil (SS) model and simulates both primary and secondary creep behaviors. The SSC model simulates time-dependent deformation, incorporates stress-level-dependent stiffness, differentiates between loading and unloading-reloading paths, employs a shear yield surface based on the Mohr-Coulomb criterion, and utilizes a volumetric yield surface based on the Modified Cam-Clay criterion. Figure 2 provides a visual representation of the yield surfaces within this model. [35].

The basis of this model is derived from the Bjerrum and Janbu theories. All non-elastic strains in this model are assumed to be time-dependent, and consequently, the total strain is the sum of elastic strain and time-dependent creep strain. The total strain equation is derived from the concept of time resistance in one-dimensional creep and is expressed as Eq. (1), capturing the relationship between creep strain and time under constant effective stress.

$$\varepsilon = \varepsilon^e + \varepsilon^c = -a \ln(\sigma'/\sigma'_0) - (b-a)\ln(\sigma_{pc}/\sigma_{p0}) - c \ln((\tau_c + t')/\tau_c) \quad (1)$$

In this equation, ε denotes the total strain, ε^e represents the elastic strain, and ε^c signifies the creep strain. σ'_0 corresponds to the initial effective stress before loading, while σ' indicates the final effective stress after loading. σ_{p0} and σ_{pc} refer to the pre-consolidation stress before loading and after consolidation is complete, respectively. The parameters a, b and c are illustrated in Figure 3. Unlike clay soils, rockfill materials do not exhibit a distinct consolidation settlement. However there exists a stress level at which the material achieves its maximum compaction. Consequently, the concept of pre-consolidation stress also utilized to characterize this behavior in rockfill materials.

The parameters κ^* (modified swelling index), λ^*(modified compression index), and μ^* (modified creep index) replace parameters a, b and c in the model respectively. The relationship between these parameters defined by Eqs. (2)-(4). The recommended values for the ratio of the compression index to the creep index range between 15 and 20, while the ratio of the compression index to the swelling index is suggested to be between 2.5 and 7 [35].

$$\kappa^* \approx 2/3\,(1+2K_0)\,a \quad (2)$$

$$\lambda^* = b \quad (3)$$

$$\mu^* = c \quad (4)$$

Figures 4 and 5 illustrate the calculation method for the aforementioned parameters in the provided diagram. In this diagram, the time at which creep begins after the consolidation period, which can be neglected for rockfill materials, is represented. Studies on rockfill materials show that the modified compression index parameter typically ranges from 2×10^{-3} to 10^{-1}, while the modified creep index ranges from 10^{-6} to 5×10^{-2}. Additionally, the ratio of the creep index to the compression index, as calculated in various studies for different types of rockfill materials, is generally reported to range from 4×10^{-3} to 5×10^{-2} [36-37].

3. Creep Model Calibration for Rockfill Materials

The validation of the SSC model for rockfill materials is carried out using data obtained from oedometer tests. In this section, the creep parameters of the dam materials are derived from two sets of oedometer tests. Subsequently, the tests were numerically simulated using the SSC model, and the outcomes of the model were compared with the experimental results. The materials used in these tests were extracted from the rockfill borrow source for Zone 3B of the downstream shell at Masjed Soleyman Dam. In the large-scale oedometer tests at the Darmstadt Research Institute [38], samples with a diameter of 1 meter and a height of 0.5 meters were subjected to axial stresses up to 2.5 MPa. The maximum particle size in these tests was 150 mm. The specimens were initially subjected to loading under dry conditions. Subsequently, saturation was obtained at three distinct axial stress levels:

2.5 MPa, 1.7 MPa, and 0.85 MPa. After saturation, loading and unloading were applied under the corresponding stress conditions. The corresponding results are presented in Figure 6 [38].

In the other tests conducted by Sadeghian [38], samples were prepared by placing materials in five layers (each layer 5 cm thick) within the inner cell of the oedometer and compacted using an electric hammer. The number of layers was selected such that the ratio of the maximum particle size to the height of each layer was 1/2, and scratches were made on the surface of each layer to ensure continuity between the layers. After preparation, a constant stress was applied to the sample by placing a weight to the device. The samples were originally made in a dry state and loaded for 24 hours. Subsequently. the samples were submerged for 7 days. The oedometer device used in these tests had a diameter of 15 cm and a height of 25 cm and the axial stresses of 0.45, 1.35, 2.25 MPa were applied to the samples [38]. The results of these tests are shown in **Error! Reference source not found.**. Figure 8 displays the particle size distribution of the materials in the test samples, as well as those from the dam shell materials.

The parameters λ^* and κ^* are calculated using the results from the Darmstadt tests. However, due to the lack of creep data in these tests, the parameter μ^* is determined from the oedometer test results reported by Sadeghian [38].

The parameters λ^* and κ^* are obtained from the loading and unloading curves in the strain versus ln(σ) diagrams for the three oedometer tests, as illustrated in Figure 9. The resulting values are summarized in Table 1.

By excluding the dry sample loading phase from the plots in Figure 7, μ^* values for different stress levels were determined from the Strain versus ln(t) diagram as illustrated in **Error! Reference source not found.**. The derived values are presented in Table .

A comparative analysis of strain-time behavior was performed between numerical simulations and experimental measurements from Sadeghian oedometer tests to validate the creep characteristics of the dam shell rockfill materials. Figure 11 validates the PLAXIS-modeled creep behavior against experimental strain-time curves from Sadeghian tests. Using the parameters specified in Table 1 and Table , the numerical simulations show consistent agreement at applied stresses of 2.25 and 1.35 MPa. While effectively simulating creep at higher stresses, the model shows divergence at 0.45 MPa. It should be noted that Sadeghian did not conduct test repetitions at stress level 0.45 MPa. Consequently, the result discrepancy may also stem from the imprecision of the single test performed at that level.

Moreover, discrepancies observed during the initial 24-hour period arise because the model parameters were calibrated exclusively for saturated conditions, while the

experimental tests included an initial dry-loading phase that was not accounted for in the numerical simulation.

4. Masjed Soleyman Rockfill Dam

Masjed Soleyman Dam is a rockfill dam with a vertical clay core and maximum height of 177 meters from the foundation. It is located 160 kilometers northeast of Ahvaz, and 25.5 kilometers northeast of Masjed Soleyman city, on the Karun River. The dam was constructed between 1997 and 2000 and the reservoir was filled in three stages, between December 2000 and August 2002. The materials used in the different parts of dam are introduced in **Error! Reference source not found.** and Table .

4-1- Modeling procedure and the model parameters

The behavior of the Masjed Soleyman Dam has been examined in many studies, including the study and modeling of saturation collapse in the dam shell [39-40], analyzing the abutment effect on the stress-strain behavior of the dam [41-42], and the examination of low-stress areas in the dam core [43].

The 2D modeling has been performed in the finite element software PLAXIS in three phases: construction, impounding, and operation. The model is plane strain and the section at 260 (the highest section of the dam) has been simulated. The foundation

of the dam is modeled only in the upper 80 meters. The meshing of the model is triangular with 5209 elements, as shown in **Error! Reference source not found.**.

To simulate the construction stage, the soil was modeled in 36 layers, with each layer being constructed over a period of 36 days. The behavior of the dam during the construction period was examined using consolidation analysis and the HS model, and the material properties are defined in Table .

During the impoundment phase, the rise in the upstream water level was modeled as a linear function, with the water level increasing over a period of 557 days. A fully coupled flow-deformation analysis was employed in this phase. Assuming that the saturation-induced collapse in the upstream shell of the dam during impoundment behaves as a form of creep, the materials were characterized using the SSC model. Additionally, the operational phase was simulated using consolidation analysis over 7300 days (20 years) with the SSC model.

The final model parameters for simulating the Masjed Soleyman Dam's behavior during impoundment and operation were obtained through a comprehensive calibration process. This involved back-analysis of laboratory test results (presented in Section 3) and field monitoring data, along with validation against observed dam performance to ensure model reliability; a parametric study was conducted to evaluate their individual influence on creep strain development in the dam model.

Accordingly, two of the three main parameters (λ^*, κ^* and μ^*) in the SSC model were held constant while the third was varied across its plausible range, allowing isolation of each parameter's effect on the time-dependent of the Dam deformation behavior. Assuming that the values of κ^*=0.00047 and μ^* =0.00006 are constant, the values of λ^* changes as shown in Figure 13-a. As observed, the variations in crest settlement over the 20-year operational period are negligible within the assumed parameter values. However, it is evident that an increase in the compression coefficient leads to a reduction in crest settlement.

Given that the values of λ^*=0.002 and μ^* =0.00006 remain constant, the values of κ^* vary as illustrated in Figure 13-b. As shown, an increase in this parameter results in an increase in settlement. Since the swelling parameter is varied over a broad range and the dam model exhibits relatively small displacement, the influence of this parameter can be considered negligible.

Assuming that the values of λ^*=0.002 and κ^*=0.00047 are constant, the values of parameter μ^* changes as shown in Figure 13-c. Initially, a rapid increase is observed, and the increment becomes more pronounced as the creep coefficient rises. Moreover, an increase in the creep coefficient causes an increase in the rate of displacement. Given the minimal changes in this parameter, it is observed that compared to the compression and swelling coefficients, this parameter has a greater effect and is the main factor for creep over time.

To understand the cause of the sudden displacement increase observed in Figure 13 and the factor affecting the slope of the deformation-time curve, the variations in the creep (μ^*) and compression (λ^*) coefficients are examined, while maintaining their ratio (μ^*/λ^*) constant. The value of κ^*=0.00047 is assumed in this section. The range of the ratio (μ^*/λ^*) considered here is based on the results of calibration with the test results in Section 3. As shown in Figure 14, if the ratio of these two parameters falls within a specific range, the sudden increase observed in Figure 13 disappears. In this regard, some sources have proposed a range for this ratio [37, 38].

The compression and swelling coefficients, determined from previous calibrations, are employed to estimate the dam parameters during the impoundment phase. To model the saturation-induced collapse in the upstream shell, the compressibility coefficient is set higher than the values derived from the oedometer tests. This discrepancy is attributed to the smaller scale of laboratory samples compared to the actual dam materials, as well as constraints related to time. Accordingly, the parameters were calibrated through an iterative trial-and-error approach by comparing 2D model results with field measurements, while incorporating the 3D valley effects as demonstrated in the 3D numerical modeling study of the dam [39].

The creep parameter in the SSC model during the operational phase is assumed to be greater than the values obtained from the oedometer tests conducted by Sadeghian [30], owing to the larger scale of the dam materials and the extended duration of

creep in the dam compared to the laboratory tests. Based on the preceding analysis, it has been established that the dam's creep behavior is independent of both the swelling and compression coefficients. Consequently, while maintaining the swelling coefficient at its experimentally determined value, the compression coefficient was increased to preserve the (μ^*/λ^*) ratio within acceptable limits, and consequently to prevent sudden discontinuities in the strain-time relationship.

Parametric sensitivity analysis across stress level reveals minimal variation in material parameters. Consequently, for modeling the Masjed Soleyman Dam shell behavior, the influence of stress level on parameter values can be neglected.

The final SSC model parameters applied during the impoundment and operational phases are as mentioned in Table .

4-2- Result of the analyses

The maximum settlement at the end of the construction of the Masjed Soleyman Dam was 3.69 m in the upper third of the dam height at the central cross-section 260. As shown in Figure -a, this value was obtained as 4.12 meters in the 2D numerical model. During the impoundment phase, the dam underwent considerable settlement caused by wetting-induced collapse in the upstream rockfill Shell. Field measurements recorded approximately 2.3 meters of settlement on the upstream side of the crest. As illustrated in Figure -b, the numerical model predicted a slightly

higher settlement of 2.9 meters at the end of the impoundment phase. Additionally, the maximum long-term settlement of the dam crest (including impoundment-induced settlement) reached approximately 5.8 meters after 20 years of monitoring. The numerical model, however, estimated a higher settlement value of 7.9 meters, as shown in Figure -c.

The displacement pattern in the model agrees well with the actual behavior observed in the dam body. The higher settlement values obtained from the numerical model—reaching up to approximately 36% in post-construction settlements—are due to the three-dimensional constraining effect of the valley topography on displacements, which is not accounted for in the current 2D model.

Considering the necessity for comprehensive parametric studies to determine the parameters of the SSC model (as presented later in this section), employing a 3D model would have required excessive time and computational costs. Thus, despite full awareness of the 3D valley effect on the dam's behavior, this study adopted a 2D modeling approach.

Micro-geodetic monitoring operations were conducted at an average frequency of once per year during the operation period of Masjed Soleyman Dam. The obtained results have been utilized as reliable data for comparison with numerical modeling outputs. The locations of the monitoring points are indicated in

Figure .

Figure and Figure display the measured settlement trends of the dam, comparing monitoring data with numerical model predictions. The figures demonstrate good agreement between the calculated and observed settlement rates, indicating the model's potential utility for forecasting future dam settlements under the assumption of continuing deformation trends. However, the model predicts settlements that are approximately 26% higher than measured values during the impoundment phase and 36% greater during the creep phase. These discrepancies are primarily attributable to the inherent limitations of two-dimensional analysis, particularly its inability to account for the constraining effects of three-dimensional valley topography.

Figure displays the total shear strain distribution in the dam body after twenty years of operation. The analysis reveals that multiple sliding surfaces have developed in both upstream and downstream zones during this period. The strain contours highlight areas of concentrated shear intensity, particularly within the downstream shell. The maximum shear strain computed in the shear zones exceeds 55%.

The high excess pore water pressure in the core remained from the construction period has reduced the effective stress and, consequently, the shear strength of the core, particularly in its central zones. The creep-induced deformation of the shells has also led to a reduction in confining stress around the central core levels. Due to

the core's relatively low resistance, this stress redistribution has generated distinct shear zones within the core structure, resulting in high shear strains in the core, according to the mechanism shown in Figure 19 [31]. The surface outcrops of these shear zones correspond to the berm formations visible in Figure, observed in both upstream and downstream shells near the crest elevation.

Notably, the numerical model shear strain contours (Figure) clearly delineate these internal shear zones within the dam body. The elevation of these modeled shear zones shows good alignment with the observed berm formations, confirming the model capability to capture the dam's deformation mechanisms.

Figure shows a comparison between the calculated and measured piezometric water level changes in the central areas of the dam section, demonstrating a reasonable agreement of the results. The plausible values of pore water pressure, alongside the comparison of settlement values, indicate the validity of the model's solution in the effective stress space during different dam loading stages.

Previous studies have demonstrated that the hyperbolic function fails to adequately predict future dam settlements, as its estimates progressively deviate from measured values. Consequently, this function proves unsuitable for reliable prediction of the dam's long-term behavior. The studies on the micro-geodetic data suggested two

functions to predict the crest settlement (S(t)) of Masjed Soleyman Dam which are introduced in Eqs. (5)-(6) [39].

$$S(t) = ab^t t^c \quad (5)$$

$$St(t) = at / (b + t) \quad (6)$$

In the above equations, *a*, *b*, and *c* represent constants derived from micro-geodetic data, and *t* denotes time in years. The results of the settlement measurements of the dam crest at section 260 based on the mentioned functions are presented in Figure . Due to the absence of geodetic measurements during the initial stages of impoundment, the model output has been time-adjusted for comparison. The red curve in the figure represents the dam crest settlement predicted by the SSC model, indicating an estimated settlement of approximately 8 meters over a 70-year period.

The discrepancy between the numerical modeling and the results obtained from the functions can be attributed to the following reasons:

1. Two-Dimensional Modeling: The use of a two-dimensional model limits the ability to capture the influence of abutments and complex valley geometry. While this approach was necessary to manage the computational cost required for the extensive parametric studies and sensitivity analyses involved in calibrating the constitutive model parameters, this simplification may

contribute to an overestimation of settlement due to the absence of three-dimensional confinement effects.

2. Estimated Parameters: A further limitation was the need to determine the model parameters from two separate sets of laboratory tests due to the unavailability of a complete dataset from a single source. This required additional computational effort for calibration and integration to achieve the necessary accuracy. On the other hand, this approach of using multiple data sources provided a higher degree of confidence in the final parameter set, as the results were cross-verified against independent experimental outcomes.

3. Exclusion of Environmental Load Effects: The effects of wet-dry cycles, changes in the reservoir water level, and material weathering were not directly incorporated into the model.

To provide a clearer overview of the adopted methodology, Figure presents a flowchart illustrating the integrated procedure followed in this study, from laboratory parameter determination to the numerical simulation and validation of the Masjed Soleyman Dam behavior.

5. Conclusion

This study investigates the creep characteristics of rockfill materials in the Masjed Soleyman Dam and assesses the efficacy of the Soft Soil Creep (SSC)

model for long-term deformation analysis of rockfill dams. The integrated procedure of laboratory testing, parameter calibration, and numerical simulation led to the following key findings and lessons learned:

- The SSC model effectively represented the developed deformation pattern and internal shear zones in the dam body, aligning with observed surface berms capturing both volumetric and shear creep mechanisms and enabled accurate simulation of time-dependent settlement patterns within the dam structure.
- Parametric studies revealed that the creep coefficient (μ^*) is the dominant parameter governing displacement rates, while the compression (λ^*) and swelling (κ^*) coefficients of the rockfill zones exhibited negligible influence. Numerical stability and realistic creep behavior require maintaining an appropriate μ^*/λ^* ratio.
- The combination of economical large-scale oedometer testing and the SSC model minimal parameters provides a practical and reliable approach for rockfill creep analysis, validated through field monitoring data that confirms result reliability.

References

[1] Zhao, Z. "DEM modeling of creep behavior of rockfill materials", *Advances in Civil, Enviromental, and Materials Research.*, Jeju Island, Korea, (2016).

[2] Wang, L., Zhu, J., Zhang, Z., et al. "Effects of dry density on shear behavior and particle breakage for slate rockfill material", *Bulletin of Engineering Geology and the Environment.*, **80**(2), pp. 1181-1192 (2020). https://doi.org/10.1007/s10064-020-01971-z

[3] Rahmani, H. and KomakPanah A. "Influence of particle size on particle breakage and shear strength of weak rockfill", *Bulletin of Engineering Geology and the Environment*., **80**, pp. 473-489, (2021). https://doi.org/10.1007/s10064-020-01889-6

[4] Soroush, A. and Jannatiaghdam R. "Behavior of rockfill materials in triaxial compression testing", *International Journal of Civil Engineering*., **10**(2), pp. 153-161, (2012).

[5] Gupta, A.K. "Effects of particle size and confining pressure on breakage factor of rockfill materials using medium triaxial test", *Journal of Rock Mechanics and Geotechnical Engineering*., **8**(3), pp. 378-388, (2016). https://doi.org/10.1016/j.jrmge.2015.12.005

[6] Chen, Q., Zhou, C. J., Wang, C., et al. "Size effect on creep behaviour and creep model of slate rockfill with oversized particles", *Proceedings of the Institution of Civil Engineers-Geotechnical Engineering*., **176**(1), pp. 3-14, (2023). https://doi.org/10.1680/jgeen.19.00296

[7] Nakata, Y., Hyodo, M., Hyde, A.F., et al. "Microscopic particle crushing of sand subjected to high pressure one-dimensional compression", *Soils and foundations*., **41**(1), pp. 69-82, (2001). https://doi.org/10.3208/sandf.41.69

[8] Zhao, Z. and Song, E.X. "Particle mechanics modeling of creep behavior of rockfill materials under dry and wet conditions", *Computers and Geotechnics*., pp. 137-146, (2015). https://doi.org/10.1016/j.compgeo.2015.04.008

[9] Zhou, X., Chi, S., Jia, Y., et al. "A probabilistic prediction method for delayed

breakage of rockfill specimens considering strength dispersion", *Computers and Geotechnics*., **184**, (2025). https://doi.org/10.1016/j.compgeo.2025.107271

[10] Guan, C., Zhang, C. and Li, C. "Influence of real particle morphology on single particle crushing behavior of rockfill based on FDEM", *Journal of Rock Mechanics and Geotechnical Engineering*., **17**, pp. 2793-2809, (2025). https://doi.org/10.1016/j.jrmge.2024.05.021

[11] Deng, G., Su, Y., Zhang, Y., et al. "Influence of Loading History on the Creep Behavior of Rockfill under Confined Oedometric Condition", *Journal of Geotechnical and Geoenvironmental Engineering*, **151**(8), (2025). https://doi.org/10.1061/JGGEFK.GTENG-12676

[12] Cetin, H., Laman, M. and Ertunc, A. "Settlement and slaking problems in the world's fourth largest rock-fill dam, the Ataturk Dam in Turkey", *Engineering geology*., **56**(3-4), pp. 225-242, (2000). https://doi.org/10.1016/S0013-7952(99)00049-6

[13] Fitzpatrick M.D., Liggins T.B. and Barnett R.H.W. "Ten years surveillance of cathana dam", *Proceedings of the 14th ICOLD Congress.*, Rio de Janeiro, pp. 847-865, (1982).

[14] Cao, K.M., Wang, Y.S. and Zhang, Z.L. "Design and construction of high concrete face rockfill dam", *Waterpower.*, **10**, pp. 49-52 (in Chinese), (2001).

[15] Zeping, X., Gang, D. and Haifang, L. "Research on creep deformation of rockfill material and post-construction deformation of rockfill dam", *Proceedings of the 17th International Conference on Soil Mechanics and Geotechnical Engineering*., (2009). https://doi.org/10.3233/978-1-60750-031-5-684

[16] Havel, F. "Creep in soft soils", doctoral thesis, *Norwegian University of Science and Technology*., (2004).

[17] Liingaard M., Augustesen, A. and Lade P.V. “Characterization of models for timedependent behavior of soils”, *Int. J. Geomech.*, **4**(3), pp. 137–156, (2004). https://doi.org/10.1061/(ASCE)1532-3641(2004)4:3(157)

[18] Li, Y., Shen, M., Du, B., et al. “An elastic-viscoplastic creep model for describing creep behavior of layered rock”, *Frontiers in Materials.*, **10**, (2023). https://doi.org/10.3389/fmats.2023.1286197

[19] Hu, A., Zhou, S., Wu, M., et al. “Modified Rheological Model for Deep-Buried Silty Mudstone and Support Time Analysis Application”, *Mathematical Problems in Engineering*., **2023**, pp. 1-16, (2023). https://doi.org/10.1155/2023/3124359

[20] Frenelus, W., Peng, H. and Zhang, J. “Creep behavior of rocks and its application to the long-term stability of deep rock tunnels”, *Applied Sciences*., **12**(17), 8451, (2022). https://doi.org/10.3390/app12178451

[21] Zhou W., Chang X.L., Zhou C.B., et al. “Creep analysis of high concrete-faced rockfill dam”, *Int. J. Numer. Methods Biomed. Eng*., **26**, pp. 1477–1492, (2010). https://doi.org/10.1002/cnm.1230

[22] Xu, M. and Song, E. “Numerical simulation of the shear behavior of rockfills” *Computers and Geotechnics*., **36**(8), pp. 1259-1264, (2009). https://doi.org/10.1016/j.compgeo.2009.05.010

[23] Varadarajan, A., Sharma, K., Venkatachalam, K., et al. “Testing and modeling two rockfill materials*”, Journal of Geotechnical and Geoenvironmental Engineering.*, **129**(3), pp. 206-218, (2003). https://doi.org/10.1061/(ASCE)1090-0241(2003)129:3(206)

[24] Varadarajan, A., Sharma, K.G., Abbas, S.M., et al. "Constitutive model for rockfill materials and determination of material constants", *International Journal of Geomechanics, ASCE*., **6**(4), pp. 226-237, (2006). https://doi.org/10.1061/(ASCE)1532-3641(2006)6:4(226)

[25] Zhang, G., Zhang, J.M., and Yu, Y. "Modeling of gravelly soil with multiple lithologic components and its application", *Soils and Foundations*., **47**(4), pp. 799-810, (2007). https://doi.org/10.3208/sandf.47.799

[26] Salim, W. and Indraratna, W. "A new elastoplastic constitutive model for coarse granular aggregates incorporating particle breakage", *Canadian Geotechnical Journal*., **41**(4), pp. 657-671, (2004). https://doi.org/10.1139/t04-025

[27] Liu, H. and Zou, D. "Associated generalized plasticity framework for modeling gravelly soils considering particle breakage", *Journal of Engineering Mechanics.*, **139**(5), pp. 606-615, (2013). https://doi.org/10.1061/(ASCE)EM.1943-7889.0000513

[28] Wen, L., Wu, L. and Li, Y. "Seepage–Creep Coupling Analysis of Concrete-Face Rockfill Dam Built on Alluvium Foundation", *International Journal of Geomechanics.*,**23**(11), (2023). https://doi.org/10.1061/IJGNAI.GMENG-894

[29] Wu, E., Zhu, J., Wang, J., et al. "Investigation on the incremental creep model of rockfill material for dam building", *Computers and Geotechnics.*,**174**(4), (2024). https://doi.org/10.1016/j.compgeo.2024.106636

[30] Liu, S., He, W., Sun, Y., et al. "Analysis of the behavior of a high earth-core rockfill dam considering particle breakage", *Computers and Geotechnics.*, **157**, (2023). https://doi.org/10.1016/j.compgeo.2023.105320

[31] Pramthawee, P., Jongpradist, P. and Sukkarak, R. “Integration of creep into a modified hardening soil model for time-dependent analysis of a high rockfill dam”, *Computers and Geotechnics*., **91**, pp. 104-116, (2017). https://doi.org/10.1016/j.compgeo.2017.07.008

[32] Sukkarak R., Pramthawee P. and Jongpradist P. “A modified Elasto-plastic model with double yield surfaces and considering particle breakage for the settlement analysis of high Rockfill dams”, *KSCE. J. Civil Eng.*, **21**(3), pp. 734–745, (2017). https://doi.org/10.1007/s12205-016-0867-9

[33] Silvani C., Désoyer T. and Bonelli S. “Discrete modelling of time-dependent rockfill behaviour”, *International journal for numerical and analytical methods in geomechanics*., **33**(5), pp. 665-685, (2009). https://doi.org/10.1002/nag.743

[34] Manso J., Marcelino J. and Caldeira L. “Crushing and oedometric deformation of rockfill using DEM”, *Congress on numerical methods in engineering*, Lisbon, Portugal, (2015).

[35] PLAXIS Manual, A.A. Balkema Publishers, Rotterdam, Printed in the Netherlands, 2002.

[36] Kermani, M. “Prediction of post-construction settlements of rockfill dams based on construction field data”, *Universite Laval*, (2016).

[37] Alonso, E., Tapias, M. and Gili, J. “Particle crushing, scale effects and delayed behaviour of rockfill. A DEM investigation”, *Alter workshop. Degradation in geomaterials*, (2013).

[38] Sadeghian, M.H., Sadeghi, M. and Fakhimi, A. “Particle breakage, deformation and shear strength of conglomerate rockfill material: a case study of Masjed Soleyman Dam cracking and settlement”, *Bull. Eng. Geo.l Environ*., **83**, 506, (2024). https://doi.org/10.1007/s10064-024-03944-y

[39] Maddah, A., Salehi, D., Fakhimi, A., et al. "Safety Evaluation and Rehabilitation Plan of Masjed Soleyman Rockfill Dam with Large Post Construction Deformations", *Bulletin of Engineering Geology and the Environment*., **84**, 494, (2025). https://doi.org/10.1007/s10064-025-04502-w

[40] Soroush, A. and Aghaei, A. "Analysis of behaviour of a high rockfill dam", *Proceedings of The Institution of Civil Engineers-geotechnical Engineering*, E. **159**, pp. 49-59, (2006). https://doi.org/10.1680/geng.2006.159.1.49

[41] Maddah, A., Soroush, A. and Tabatabaie Shourijeh, P. "Effects of material properties on behavior of embankment dam clay cores in narrow valleys", *Scientia Iranica*., **22**, pp. 1692-1702, (2015).

[42] Soroush, A., Pourakbar, M. and Nabizadeh, A. "3D numerical analyses of behavior of a high rockfill dam with clay core in narrow canyon", *Proceeding of 16th Asian Regional Conference on Soil Mechanics and Geotechnical Engineering.*, (2019).

[43] Pourakbar, M., and Soroush, A. "Low Stress Zones in Core of High Rockfill Dam using 3D Analyses", *Proceedings of the 19th International Conference on Soil Mechanics and Geotechnical Engineering*, (2017).

Biographies

Yasaman Delavar Rafie is a master's graduate in Geotechnical Engineering from Amirkabir University of Technology. Her work focuses on geotechnics, dam engineering, and numerical modeling. She is particularly interested in applying computational methods to improve geotechnical design and analysis.

Dr. Arman Maddah is an Assistant Professor and faculty member at Amirkabir University of Technology (Tehran Polytechnic). His primary research focuses on the monitoring, behavioral modeling, back-analysis, and remediation of geotechnical structures. This expertise specifically encompasses earth and rockfill dams, deep excavations, and underground spaces such as caverns.

Professor Abbas Soroush is a Full Professor and faculty member of the School of Civil and Environmental Engineering at Amirkabir University of Technology (Tehran Polytechnic) and currently serves as the President of the university. His specialization lies in geotechnical structures such as earth dams, Tunneling and deep excavations, as well as environmental geotechnics. He has authored over 160 articles with about 2500 citations. The engineering of earth dams is also among his professional interests, having supervised the design, construction, and rehabilitation of many large dams in the country.

Figure Captions

Figure 1- Different phases of creep in geotechnical materials [13]

Figure 2- yield surfaces of SSC model [35]

Figure 3- Ideal stress-strain curve from oedometer test with separation of elastic and creep strains [35]

Figure 4- Definition of the modified compression index and modified swelling index parameters using a standard oedometer test [35].

Figure 5- Introduction of the modified creep index parameter using a standard oedometer test in the diagrams: a) creep strain versus logarithmic time, b) inverse creep strain rate versus time [35].

Figure 6- Stress-strain diagram of large-scale oedometer tests on the materials from the Masjed Soleyman Dam shell at Darmstadt Institute [38].

Figure 7- Strain-time diagram of oedometer tests on the materials from the Masjed Soleyman Dam shell [38].

Figure 8- Comparison of the particle size distributions in Sadeghian and Darmstadt test samples and the dam shell materials [38]

٥٥٢ Figure 9- Calculation of the model parameters based on oedometer test results: a) Modified compression index (λ^*)
٥٥٣ b) Modified Swelling index (κ^*)

٥٥٤ Figure 10- Saturated-phase strain-time curves from oedometer tests (Sadeghian, 2024) for modified creep index
٥٥٥ parameter (μ^*) calculation in Masjed Soleyman Dam shell materials.

٥٥٦ Figure 11- Comparison of creep behavior between experimental results and Soft Soil Creep (SSC) model
٥٥٧ simulations of Sadeghian (2024) oedometer tests on rockfill materials at $\sigma' = 0.45$, 1.35, and 2.25 MPa.

٥٥٨ Figure 12- a) Zoning and mesh generation of the Masjed Soleyman main dam section model, b) Valley cross-section
٥٥٩ at the dam site [41]

٥٦٠ Figure 13- Effect of model parameters on the creep strain of the dam crest at section 260 over time a) Compression
٥٦١ coefficient, b) Swelling coefficient, c) Creep coefficient

٥٦٢ Figure 14- Comparison of crest settlement over time for an approximately constant ratio of creep coefficient to
٥٦٣ compression coefficient ($\mu^*/\lambda^* \approx 0.08$-0.09)

٥٦٤ Figure 15- Contours of settlement in the Dam a) During construction phase b) During impoundment phase c) During
٥٦٥ impoundment and 20 years of operation phases

٥٦٦ Figure 16- Geodetic network on the Masjed Soleyman dam; 25 target points installed on the crest and downstream
٥٦٧ surface at various cross-sections [39]

٥٦٨ Figure 17- Validation of numerical model results against field monitoring data: Comparison of simulated and
٥٦٩ measured crest settlement at instrumentation point S21

٥٧٠ Figure 18- Validation of numerical model results against field monitoring data: Comparison of simulated and
٥٧١ measured settlements at downstream shell instrumentation points a) S22 b) S23 c) S24 d) S25

٥٧٢ Figure 19- Creep phase shear strain at section 260 calculated 20 years after impoundment

٥٧٣ Figure 20- Manifestation of shear zones as surface berms: a) Downstream (D/S) slope of the dam, and b) Upstream
٥٧٤ (U/S) slope of the dam [40]

٥٧٥ Figure 21- Comparison of calculated and measured piezometric water level in piezometer PPE 213

Figure 22- Predicted settlement trends of the dam crest using microgeodetic data compared with the calculated results

Figure 23- Flowchart illustrating the research methodology, including laboratory parameter calibration, numerical modeling stages, and validation against field data in this study.

Table Captions

Table 1- Modified compression (λ^*) and swelling (κ^*) indices obtained from large-scale oedometer tests (Darmstadt Institute).

Table 2- The calculated values of modified creep index parameter μ^* in different stresses

Table 3- Materials used in different zones of the body of the Masjed Soleyman Dam [39]

Table 4- Parameters of the Masjed Soleyman Dam Model [39]

Table 5- Creep and compression coefficients with a relatively constant ratio

Table 6- Creep parameters in different zones of the shell of Masjed Soleyman Dam during the first impoundment and operation stages

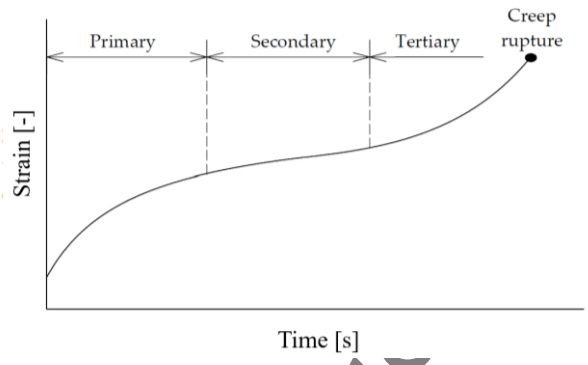

Figure 1

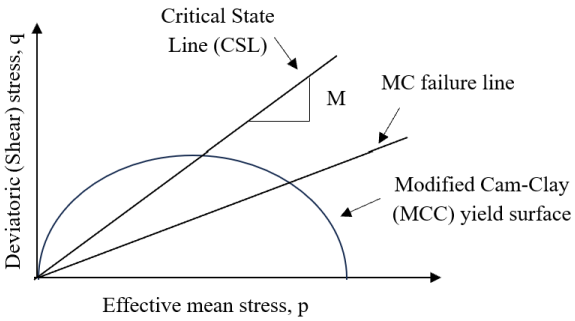

Figure 2

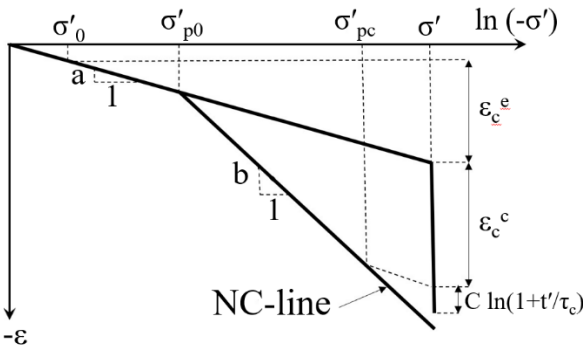

٦١٠
٦١١

Figure 3

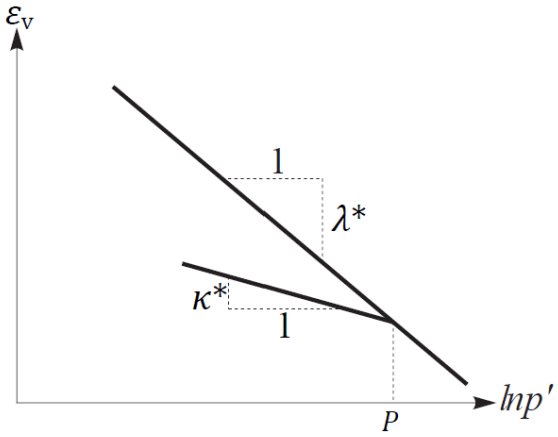

٦١٢
٦١٣

Figure 4

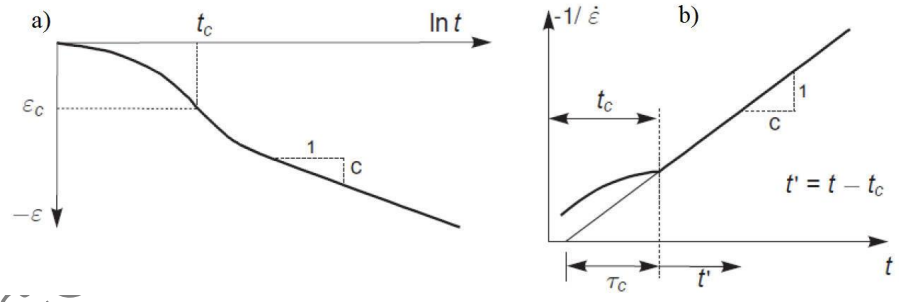

٦١٤

٦١٥

Figure 5

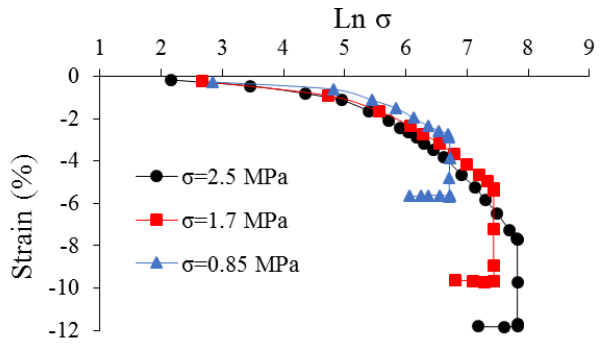

٦١٦

٦١٧

Figure 6

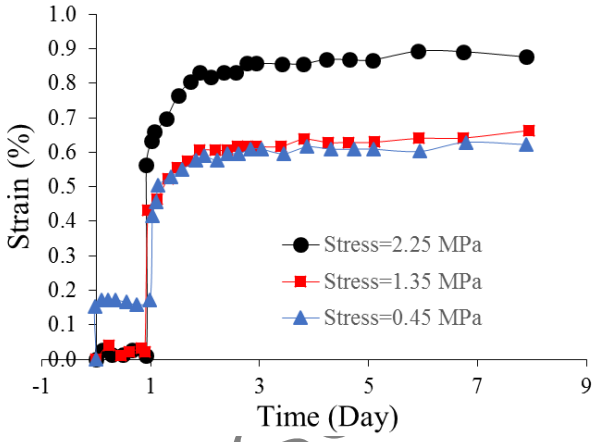

٦١٨

٦١٩

Figure 7

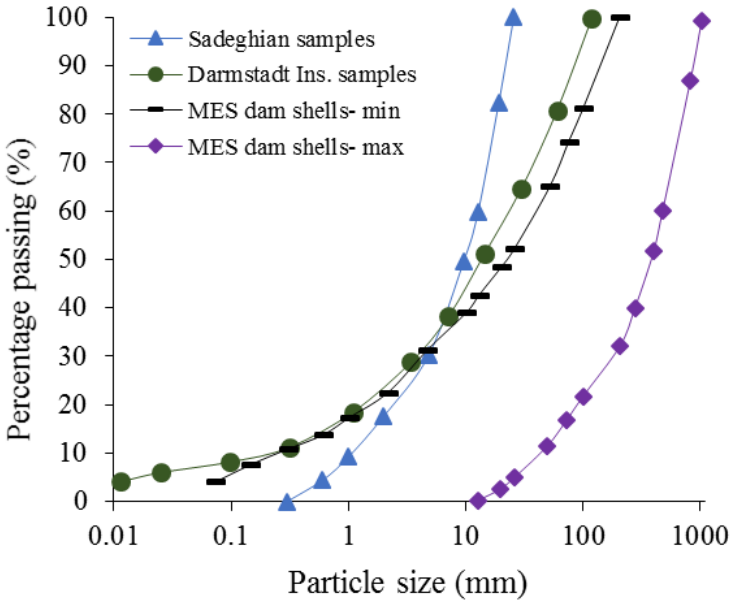

٦٢٠

٦٢١

Figure 8

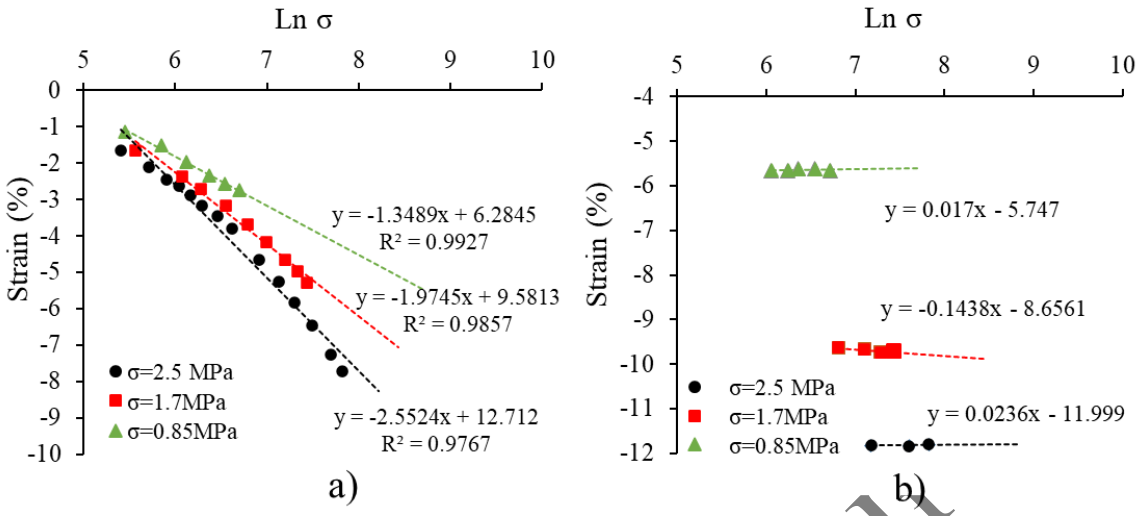

٦٢٢

٦٢٣

Figure 9

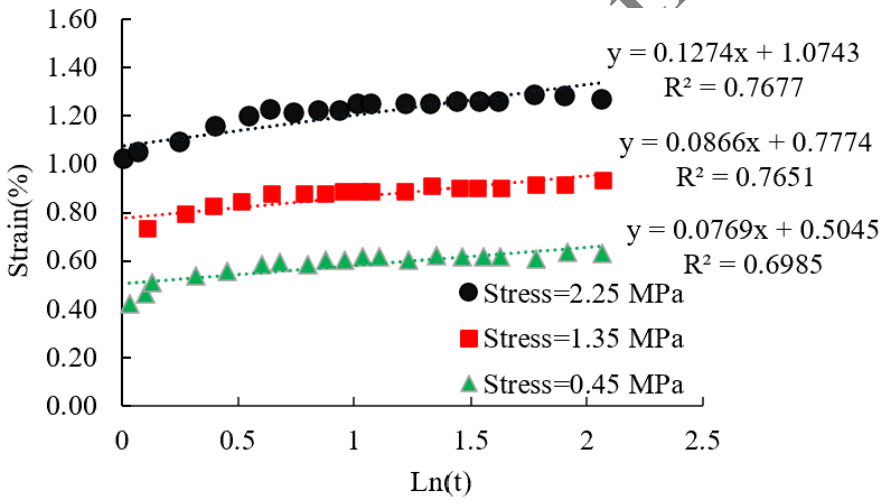

٦٢٤

٦٢٥

Figure 10

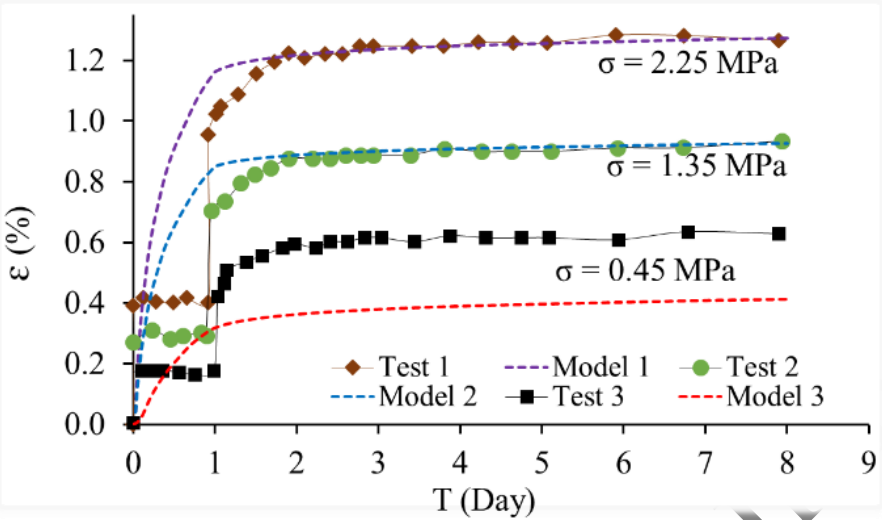

٦٢٦

٦٢٧ Figure 11

٦٢٨

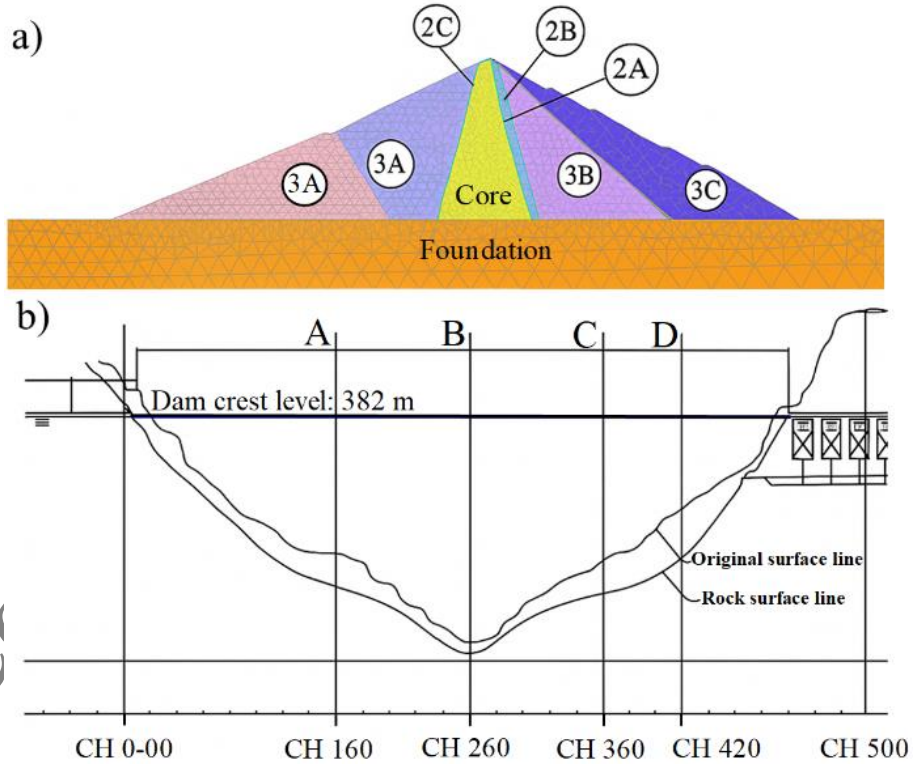

٦٢٩

٦٣٠ Figure 12

٦٣١

٦٣٢

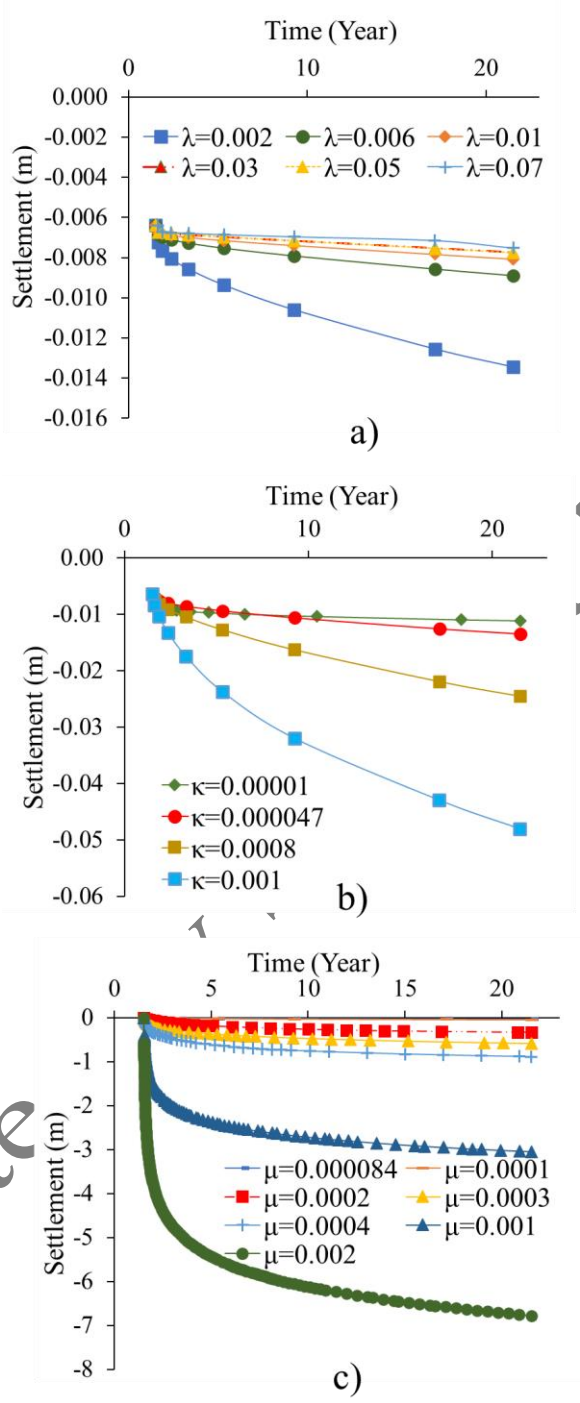

٦٣٣

٦٣٤ Figure 13

٦٣٥

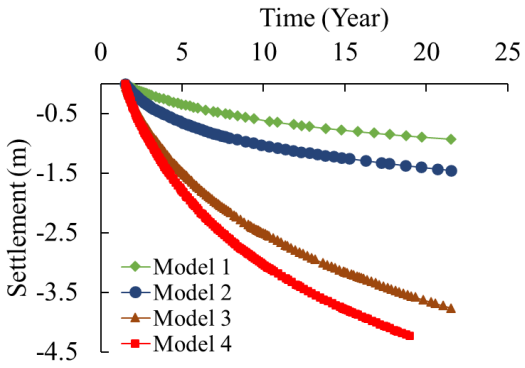

٦٣٦

٦٣٧ Figure 14

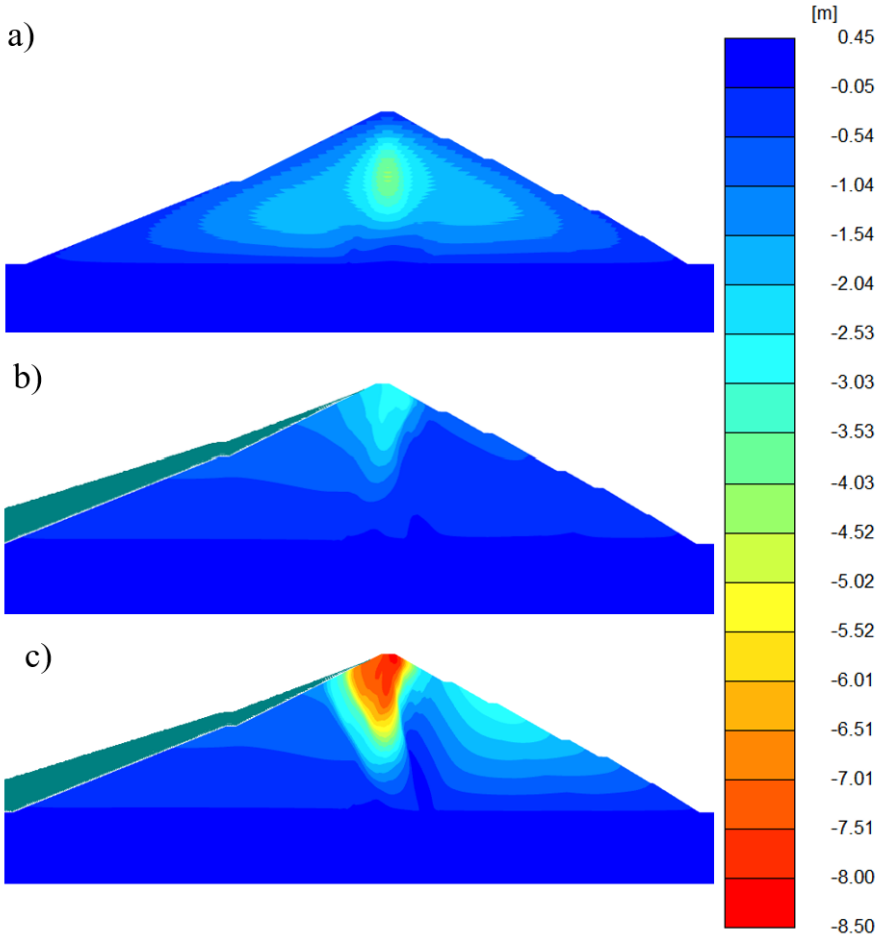

٦٣٨

٦٣٩ Figure 15

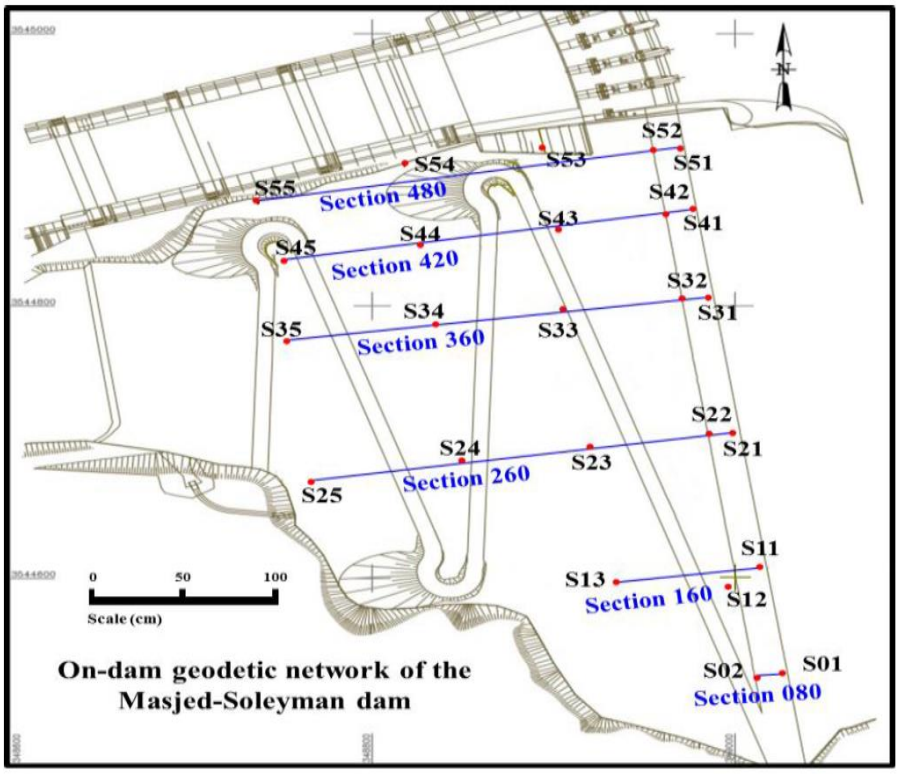

Figure 16

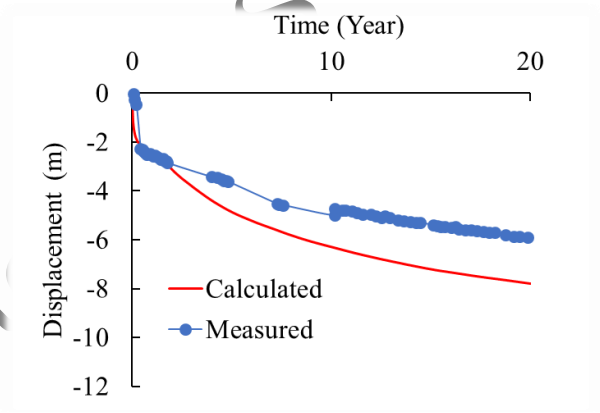

Figure 17

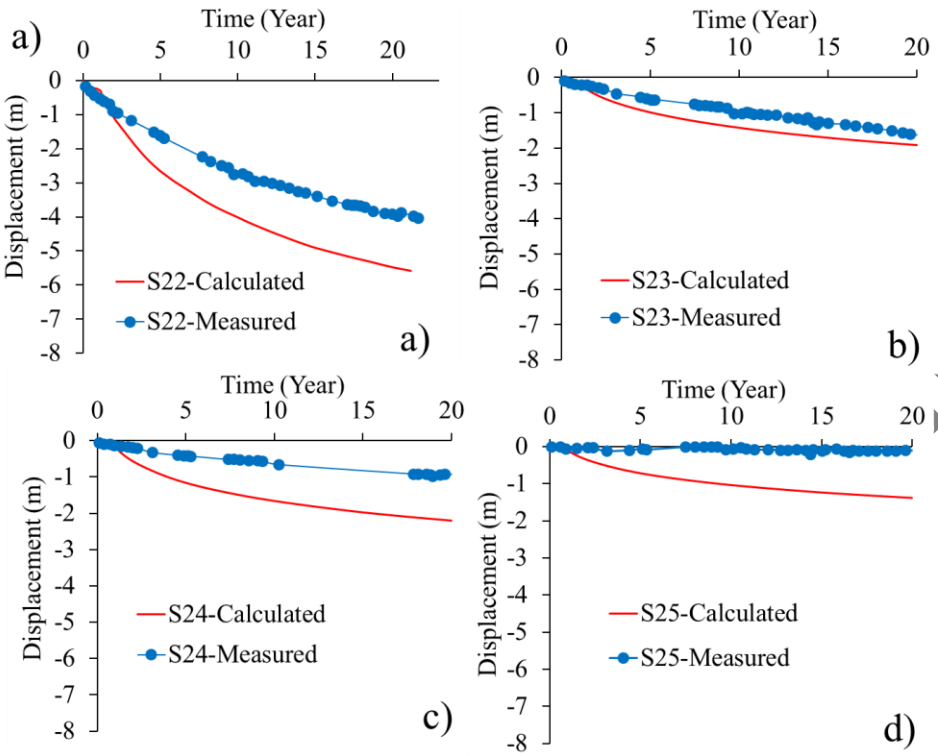

٦٤٤

٦٤٥ Figure 18

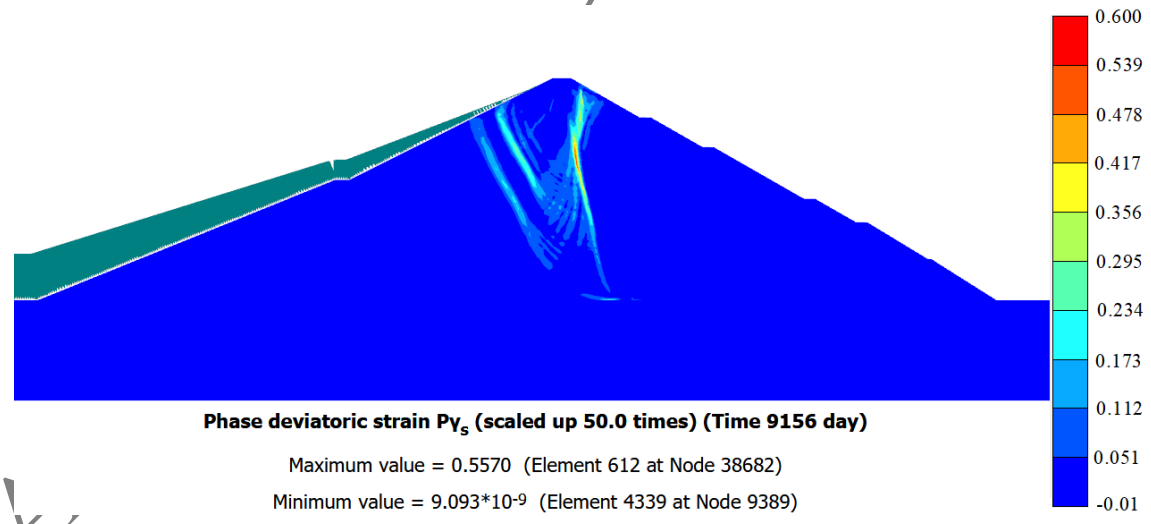

٦٤٦

٦٤٧ Figure 19

٦٤٨

Figure 20

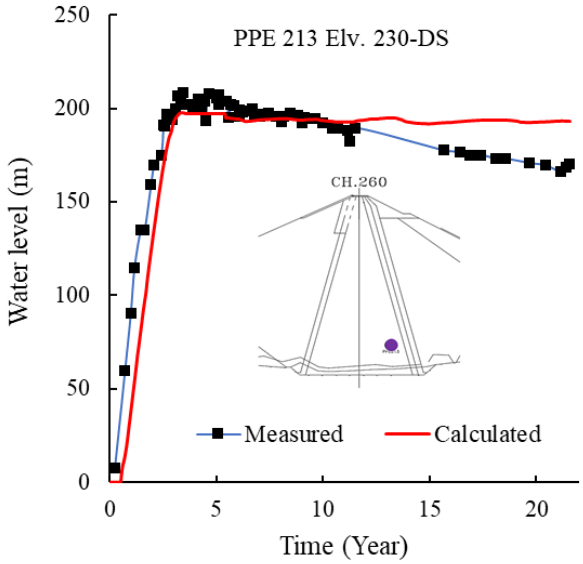

Figure 21

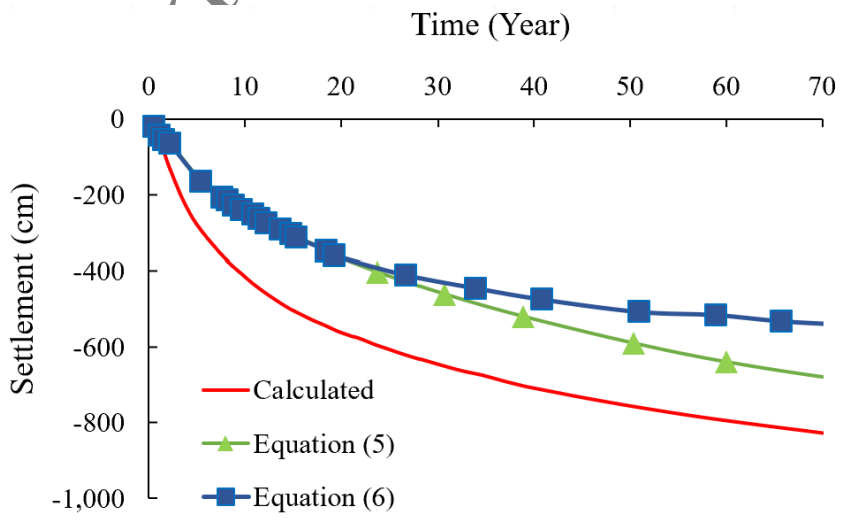

Figure 22

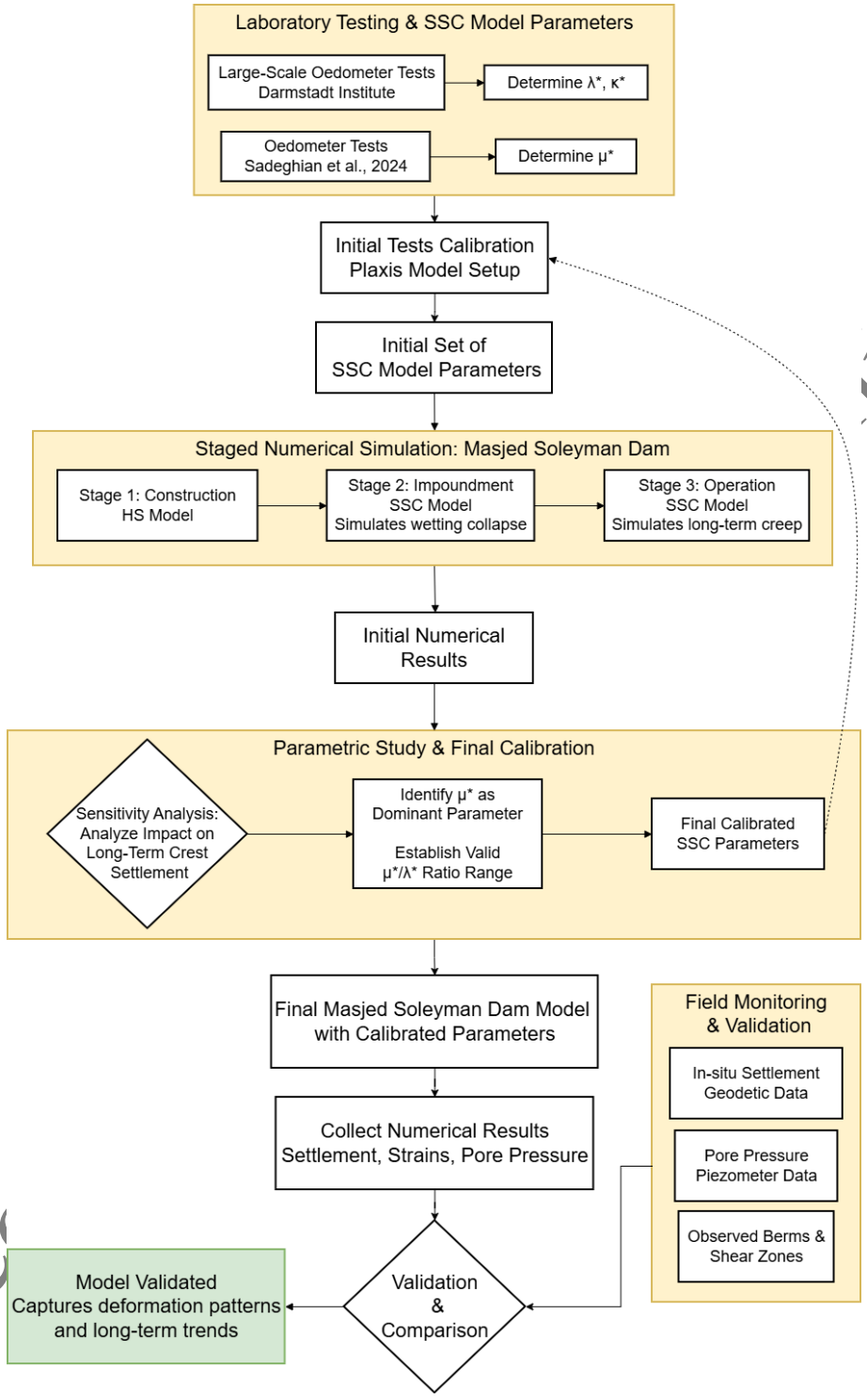
Laboratory Testing & SSC Model Parameters
Large-Scale Oedometer Tests
Darmstadt Institute
Determine λ*, κ*
Oedometer Tests
Sadeghian et al., 2024
Determine μ*
Initial Tests Calibration
Plaxis Model Setup
Initial Set of
SSC Model Parameters
Staged Numerical Simulation: Masjed Soleyman Dam
Stage 1: Construction
HS Model
Stage 2: Impoundment
SSC Model
Simulates wetting collapse
Stage 3: Operation
SSC Model
Simulates long-term creep
Initial Numerical
Results
Parametric Study & Final Calibration
Sensitivity Analysis:
Analyze Impact on
Long-Term Crest
Settlement
Identify μ* as
Dominant Parameter
Establish Valid
μ*/λ* Ratio Range
Final Calibrated
SSC Parameters
Final Masjed Soleyman Dam Model
with Calibrated Parameters
Field Monitoring
& Validation
In-situ Settlement
Geodetic Data
Pore Pressure
Piezometer Data
Observed Berms &
Shear Zones
Collect Numerical Results
Settlement, Strains, Pore Pressure
Validation
&
Comparison
Model Validated
Captures deformation patterns
and long-term trends

Figure 23

Table 1

Number	Applied stress (MPa)	λ^*	κ^*
1	2.5	0.0255	0.000472
2	1.7	0.019	0.002876
3	0.85	0.01348	0.000894

Table 2

Number	Applied stress (MPa)	μ^*
1	2.25	0.001274
2	1.35	0.000866
3	0.45	0.000769

Table 3

Zone	Symbol	Material
Core	1	Clay
Fine-grained Filter	2A	Conglomerate with fine and coarse sand
Coarse-grained Filter	2B	Conglomerate with coarse to medium gravel
Transition materials	2C	Conglomerate with fine rockfill
Rockfill shell	3A	Conglomerate
Rockfill shell	3B	Conglomerate mixed with sandstone and intrusive bodies of mudstone / clay-bearing mudstone
Rockfill shell	3C	Conglomerate mixed with sandstone
Foundation	4	Mudstone and shale and the sequence of conglomerate and sandstone

٦٦٧ Table 4

Zone	K_0	m	P_{ref} (kPa)	ψ (˚)	φ' (˚)	c' (kPa)	E_{ur}^{ref} (MPa)	E_{oed}^{ref} (MPa)	E_{50}^{ref} (MPa)	k (cm/s)	γ_{sat} (kN/m^2)	e_0
2A	0.43	0.5	100	2	39	10	75	12	22	5.8×10^{-3}	22	0.42
2B	0.36	0.5	100	6	40	20	120	18	40	4.6×10^{-3}	21.2	0.52
2C	0.43	0.5	100	2	39	10	75	12	22	5.8×10^{-3}	22	0.42
Core	0.52	0.35	100	0	22	80	33	11	11	5×10^{-9}	21.7	0.43
3A	0.34	0.15	100	3.5	38	70	180	38	60	9.8×10^{-3}	24.2	0.2
3B	0.6	0.17	100	1	31	30	130	45	45	1×10^{-2}	24.2	0.2
3C	0.34	0.15	100	3.5	38	70	180	38	60	9.8×10^{-3}	24.2	0.2
Foundation	-	-	-	6	40	700	45	-	7500	1×10^{-9}	25	-

٦٦٨

٦٦٩ Table 5

Model No.	λ^*	μ^*	μ^*/λ^*
1	0.025	0.002	0.08
2	0.028	0.0025	0.089
3	0.0625	0.005	0.08
4	0.08	0.007	0.087

٦٧٠

٦٧١

٦٧٢ Table 6

Zone	Stage	λ^*	κ^*	μ^*
3A	Impoundment	1×10^{-1}	4.7×10^{-4}	9×10^{-3}
	Operation	1.5×10^{-2}	4.7×10^{-4}	2×10^{-3}
3B	Impoundment	1×10^{-1}	4.7×10^{-4}	9×10^{-3}
	Operation	$1.3*10^{-2}$	4.7×10^{-4}	1.5×10^{-3}
3C	Impoundment	1×10^{-1}	4.7×10^{-4}	9×10^{-3}
	Operation	$1.3*10^{-2}$	4.7×10^{-4}	1.5×10^{-3}

٦٧٣

٦٧٤